J Mater Sci: Mater Med (2009) 20:1009–1015
DOI 10.1007/s10856-008-3662-4

Influence of hydroxyapatite on the corrosion resistance of the Ti-13Nb-13Zr alloy

Laís T. Duarte · Sonia R. Biaggio · Romeu C. Rocha-Filho · Nerilso Bocchi

Received: 6 August 2008 / Accepted: 2 December 2008 / Published online: 13 December 2008

Abstract Electrochemical analyses on the biocompatible alloy Ti-13Nb-13Zr wt% in an electrolyte simulating physiological medium (PBS solution) are reported. Hydroxyapatite (HA) films were obtained on the alloy by electrodeposition at constant cathodic current. Samples of the alloy covered with an anodic-oxide film or an anodic-oxide/HA film were analyzed by open circuit potential and electrochemical impedance spectroscopy measurements during 180 days in the PBS electrolyte. Analyses of the open-circuit potential (E_{oc}) values indicated that the oxide/HA film presents better protection characteristics than the oxide only. This behavior was corroborated by the higher film resistances obtained from impedance data, indicating that, besides improving the alloy osteointegration, the hydroxyapatite film may also increase the corrosion protection of the biomaterial.

1 Introduction

Titanium, niobium, and zirconium, belonging to a group known as valve metals, usually have their surfaces covered by a thin oxide film spontaneously formed in air or in electrolytic solutions at open circuit [1, 2]. This oxide film constitutes a barrier between the metal and the medium. When formed in air at room temperature, these oxides present thicknesses in the range 2–5 nm, which can be increased by anodic oxidation [1–3] leaving the metallic material in the so-called passive state. Currently, there is a growing need for the use of artificial implants, which makes necessary more thorough studies on materials that may be used for such application [4–6]. A live organism, containing saline solutions, is considered to be a corrosive medium for several materials; due to the high corrosion resistance of valve metals in different highly corrosive environments (mainly those of an oxidative nature or containing chlorides) [7], the field for application of these metals and their alloys is naturally enlarged, allowing rapid and significant advances in the areas of medical instrumentation and surgical implants [8]. Considering that some Ti alloys present, among other qualities, excellent mechanical properties, very good corrosion resistance and biocompatibility, beside good durability, they become promising materials for use in implants [9].

Some potentially biocompatible alloys have been intensively studied with a strong emphasis on their corrosion behavior, surface properties, and biocompatibility in implants [9–14]. As pointed out by López et al. [10], a detailed knowledge of the surface composition of new biomaterials is essential because the most outer layers are in direct contact with biological tissues. Khan et al. [11] called the attention to the fact that the Ti-13Nb-13Zr alloy, vanadium-free and made of non-toxic elements, was proposed as more favorable for orthopaedic implants than the Ti-6Al-4V alloy because of its superior corrosion resistance and biocompatibility. Khan et al. [12] also compared the corrosion resistance of a variety of alloys, including the Ti-13Nb-13Zr alloy, in a phosphate buffered saline (PBS) solution at three different pHs. They concluded that this alloy was among the ones presenting the best corrosion resistance properties, along with commercially pure Ti and the Ti-15Mo alloy.

L. T. Duarte · S. R. Biaggio (✉) · R. C. Rocha-Filho · N. Bocchi
Departamento de Química, Universidade Federal de São Carlos, C.P. 676, 13560-970 Sao Carlos, SP, Brazil
e-mail: biaggio@ufscar.br

López et al. [10] analyzed X-ray photoelectron spectroscopy (XPS) spectra carried out on the oxide layers formed spontaneously in air on three vanadium-free Ti alloys: Ti-6Al-7Nb, Ti-13Nb-13Zr, and Ti-4Nb-15Zr. The XPS data revealed for these alloys a passive layer formed by a mixture of the oxides from the respective elements, but largely enriched in Al or Zr oxides. They also reported on the behavior of the same titanium alloys in Hank's solution [13]: no transpassivation was recorded and no pit formation was evident at potentials as high as 2 V (vs. saturated calomel electrode (SCE)).

Studies done in our laboratory [14–17] on the stability of oxides grown anodically on Ti-50Zr at.%, Zr-2.5Nb wt%, and Ti-13Nb-13Zr wt%, in aerated *Ringer* physiological solutions, showed that the stability of these oxides is increased by aging under potentiostatic conditions and can be decreased by the presence of chloride ions in the electrolyte during the anodization process. We also reported that, in some solutions simulating physiologic media [Ringer and PBS (phosphate buffered saline) solutions], the Ti-50Zr alloy presents a better corrosion protection than the Zr-2.5Nb alloy or pure Zr [15]. Furthermore, the anodized Ti-13Nb-13Zr alloy did not present any corrosion evidence even at potentials as high as 8 V (vs. SCE) in chloride solutions, while the Ti-50Zr alloy underwent localized corrosion (pit corrosion) at potentials lower than 2 V [17]. Besides that, we showed that the dissolution of the oxide grown anodically on the Ti-13Nb-13Zr alloy, measured after 3 days of immersion in PBS solution at open circuit, was only about 3%, which is very low compared to the dissolution presented by the oxides of the other alloys [17].

In order to increase their biocompatibility, these oxidized alloys have been coated with biocompatible ceramics, which can be used in either orthopaedic or dental implants. Among the bioactive materials are the bioglasses, the glass ceramics and the calcium–phosphate-type ceramics, the latter group having hydroxyapatite (HA, $Ca_{10}(PO_4)_6(OH)_2$) as their most widely employed material [18, 19]. The coating of an implant material with HA is especially attractive since it is the main mineral component of the bone and results in improved osteointegration when placed in the metal/living tissue interface [20–24].

Several methods have been employed in order to prepare HA coatings; the plasma spraying method is the most reported. Nevertheless, it is not an easy task to precisely control the chemical composition, crystallographic phase, and thickness of the deposited material by using this technique. A good alternative is to use electrochemical deposition to quickly obtain uniform HA coatings on substrates of complex shapes at room temperature, besides allowing the control of the thickness and the composition of the film [23].

Several reports can be found on the HA electrodeposition on a Ti substrate using different compositions of the forming electrolyte containing calcium and phosphate salts [21–24]. However, not as many reports can be found on HA deposition on the promising Ti-13Nb-13Zr alloy. Besides that, there is also very little information concerning the changes on the electrochemical properties when a metallic biomaterial is coated with HA and what important aspects can be analyzed on the alloy/HA/electrolyte interfaces by means of electrochemical techniques. Therefore, the aim of this work was to investigate the effect of an HA coating on the electrochemical properties of the Ti-13Nb-13Zr alloy passivated by its oxide. To accomplish this, a methodology to electrodeposit HA on the fresh-polished alloy was firstly optimized and then, the apatite film was electrodeposited using the same procedure on the Ti-13Nb-13Zr surface already passivated by an oxide film grown anodically. The stability and the corrosion behavior of the alloy/oxide and alloy/oxide/HA samples, kept in a PBS solution, were followed during 180 days by means of open-circuit potential and electrochemical impedance spectroscopy (EIS) measurements.

2 Experimental

The Ti-13Nb-13Zr wt% alloy was prepared by voltaic-arc fusion in an inert atmosphere of the pure metals (Zr 99.8%, Nb 99.8%, and Ti 99.7%, from Aldrich), following a procedure described by Kobayashi et al. [9]. The obtained alloy was characterized by metallography and by inductively coupled plasma-atomic emission spectroscopy (ICP-AES) [17].

Working electrodes were made from disk-shape pieces of the Ti-13Nb-13Zr alloy exposing a geometrical area of about 1 cm^2 to the electrolyte. Previous to any HA or anodic oxide growth, the alloy surface was polished with grade-600 silicon carbide paper and rinsed with deionized (Milli-Q®) water. A conventional three-electrode cell was used in all the electrochemical experiments and the solutions were always kept at room temperature, *ca.* 25°C. A saturated calomel electrode was used as reference and a 2-cm^2 Pt foil was used as counter electrode.

The oxides were grown on the surface of the Ti-13Nb-13Zr electrode at constant anodic current density (1.52 mA cm^{-2}) up to 80 V, in a pH 5 phosphate solution (35.81 g/l Na_2HPO_4, 13.80 g/l NaH_2PO_4) as electrolyte. This procedure yields an anodization ratio of about 2 nm V^{-1}, according to our previous results [17].

The hydroxyapatite was electrodeposited on the fresh-polished alloy by applying −13 mA cm^{-2} during 60 min in an electrolyte containing 137.8 mmol/l NaCl, 1.67 mmol/l K_2HPO_4, and 2.5 mmol/l $CaCl_2$ [24]. The

same procedure was employed to electrodeposit HA on the alloy passivated by its 80-V oxide. The morphology and the structure of the coated alloy surface were analyzed, respectively, by a Zeiss DSM 960 scanning electron microscope and a Rigaku Rotaflex RU200B X-ray diffractometer.

Several samples of the Ti-13Nb-13Zr alloy, coated with either its anodic oxide or anodic oxide/HA films, were left in an aerated PBS solution during 180 days at room temperature. From time to time, one sample had its electrochemical properties analyzed as follows: (a) open-circuit potential (E_{oc}) measurements carried out in the PBS solution; (b) EIS measurements carried out in the same solution keeping the alloy electrode at 2 V (in the oxide stability region, in order to establish high signal-to-noise ratio and data stability). For the EIS measurements, a sinusoidal signal of 10 mV (rms) was applied in the frequency range 10 mHz–10 kHz, using an Autolab PGSTAT30 potentiostat/galvanostat from Eco Chemie controlled by the FRA software. The fitting of an equivalent electrical circuit model to the impedance data was done using a non-linear least square method.

3 Results and discussion

3.1 Electrochemical deposition of hydroxyapatite on the alloy and alloy/oxide surfaces

From aqueous solutions containing calcium and phosphate ions, a calcium phosphate film similar to the bone hydroxyapatite can be deposited on metallic surfaces mediated by the cathodic reduction of water

$$2H_2O + 2e^- \rightarrow H_2(aq) + 2OH^-(aq) \quad (1)$$

since the increase of the pH at the metal/solution interface induces the precipitation of calcium phosphate salts as an insoluble and adherent layer on the cathode, as proposed before [25–27]:

$$OH^-(aq) + H_2PO_4^-(aq) \rightarrow HPO_4^{2-}(aq) + H_2O(l) \quad (2)$$

$$OH^-(aq) + HPO_4^{2-}(aq) \rightarrow PO_4^{3-}(aq) + H_2O(l) \quad (3)$$

$$2OH^-(aq) + 6PO_4^{3-}(aq) + 10Ca^{2+} \rightarrow Ca_{10}(PO_4)_6(OH)_2(s) \quad (4)$$

Accordingly, the formation of the hydroxyapatite (HA) film on fresh-polished Ti-13Nb-13Zr samples was analyzed as a function of the electrodeposition time. Figure 1 shows how the hydroxyapatite mass changed with time for two cathodic current density values, -13 mA cm^{-2} and -15 mA cm^{-2}, until the film reached a constant mass value. This current density range was elected since for higher values the hydrogen evolution rate (Eq. 1) is very high, negatively affecting the quality of the HA deposit, while for lower values the co-deposition of dicalcium-phosphate dihydrate is favored [27]. The obtained results indicate that 60 min is an optimum time to reach a steady amount of the HA film, which does not vary significantly with the cathodic current employed. Therefore, the subsequent HA depositions were done during 60 min at -13 mA cm^{-2}.

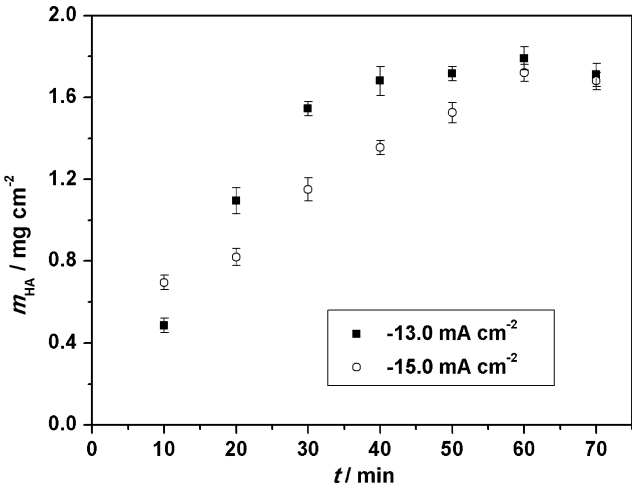

Fig. 1 Hydroxyapatite mass versus electrodeposition time for two different cathodic current densities (values are averages of three experiments)

The surface aspect of the Ti-13Nb-13Zr alloy covered with an electrodeposited HA film was analyzed by scanning electron microscopy (SEM) and the film structure by X-ray diffractometry (XRD); typical results are presented in Fig. 2. The micrograph at lower magnification (Fig. 2a) displays a continuous and homogeneous film distributed on the alloy surface, while the one at higher magnification (Fig. 2b) reveals a globular and porous film. The porosity obtained for the electrodeposited hydroxyapatite is a positive feature for the implanted material since it favors both osteointegration [19, 28, 29] and drug delivery through it [29, 30]. The X-ray diffractogram, shown in Fig. 2c, reveals main peaks at $2\theta \sim 26$, 32 and 34 degrees, which are compatible to HA peaks [31–33]. Simultaneously to the SEM analyses, an elemental determination was carried out by EDS in order to quantify the Ca/P ratio in the HA film. The relative percentages yielded by the corresponding peak areas were 61.7% for calcium and 38.3% for phosphorous, leading to a Ca/P ratio of 1.61, which is very close to the bone hydroxyapatite value (Ca/P = 1.67). This is an excellent result specially when considering that the HA film was prepared at room temperature, without the need of further sintering usually performed to obtain HA by other methodologies [18, 19].

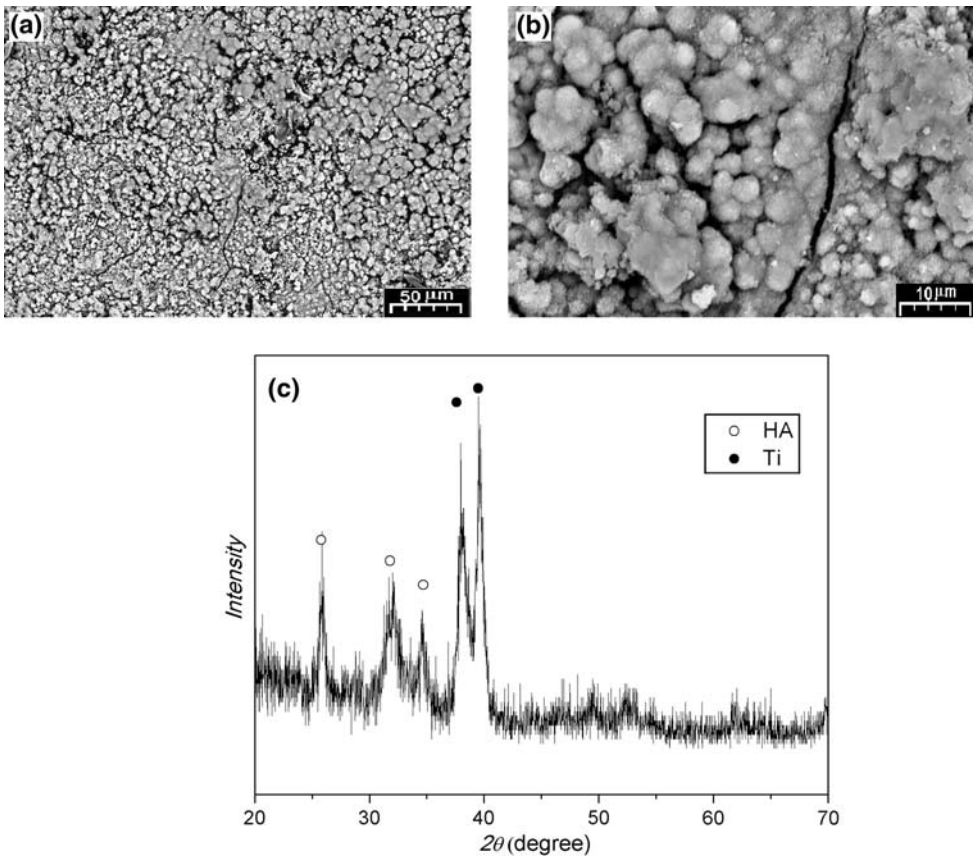

Fig. 2 SEM micrographs at two magnifications (**a**) and (**b**) and X-ray diffractogram (**c**) of the hydroxyapatite film electrodeposited on the Ti-13Nb-13Zr alloy

The same procedure was carried out to electrodeposit HA on the alloy already passivated by its oxide grown up to 80 V. The growth and characterization of this oxide on the Ti-13Nb-13Zr alloy were analysed in detail previously [14, 16, 17]. Considering the anodization ratio of the alloy as 2 nm V^{-1}, the thickness of the oxide passivating the alloy was estimated as approximately 160 nm. The micrograph shown in Fig. 3 indicates that the morphology of the HA film is completely changed when it is deposited on this thick and rather compact oxide film. Due to the resistance imposed by the anodic oxide film, only a very thin layer of HA was expected to be deposited on the alloy/oxide electrode. Hence, the surface aspect of the oxide/HA film seems to be similar to that of the underlying oxide [14, 16, 17].

Although the XRD and EDS analyses for the alloy/oxide/HA samples were non-conclusive, i.e. very small signals of the corresponding peaks (not shown in this paper) due to the low HA thickness, the presence of the apatite film on the oxide was attested by the variation of the alloy/oxide properties as analyzed in the sequence.

3.2 Characterization by open circuit potential and EIS measurements

Open-circuit potential (E_{oc}) analyses have been widely used to foresee the corrosion or passivity properties of various alloys used as biomaterials [20, 34]. Figure 4 presents the E_{oc} variation of the Ti-13Nb-13Zr alloy immersed in a PBS solution during 180 days, for samples coated with either its anodic oxide film or HA overlaying this oxide film. For both cases, E_{oc} varies significantly at the beginning till the equilibrium potential is reached in the PBS electrolyte; then, it varies slowly towards lower potentials till an approximately steady value is reached.

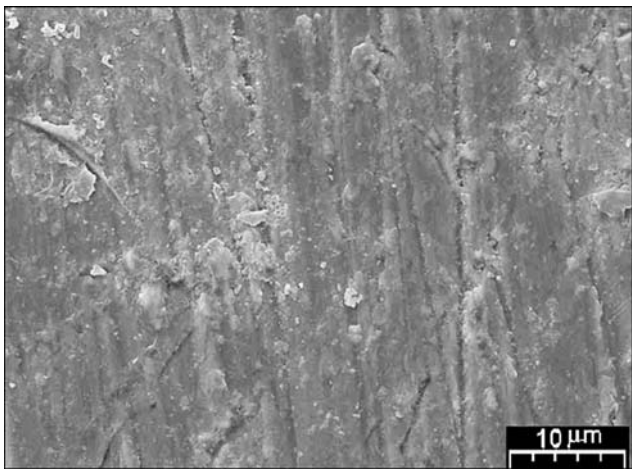

Fig. 3 SEM micrograph of the hydroxyapatite film electrodeposited on the Ti-13Nb-13Zr alloy passivated by a 80-V oxide

Two important informations can be drawn from these results: first, the slow drift of E_{oc} towards more negative (and quasi-stationary) values is an indication that a small dissolution rate (tending to a negligible equilibrium value) is taking place at the film/solution interface; second, the higher E_{oc} values (upper curve in Fig. 4) obtained for the alloy/oxide/HA electrode indicate that this system presents less tendency to spontaneously undergo dissolution in the PBS solution. Therefore, it seems that the presence of the HA film affects the stability and offers additional corrosion protection to the already passive underlying alloy.

Electrochemical impedance spectroscopy (EIS) measurements were performed in order to complement the analyses of the electrochemical properties of the passive Ti-13Nb-13Zr alloy. To do so, EIS spectra were obtained for the alloy/oxide and alloy/oxide/HA electrodes as a function of the immersion time in the PBS solution. Typical results are shown in Figs. 5 and 6 for the alloy/oxide and alloy/oxide/HA electrodes, respectively. The impedance profiles for the passive alloy electrodes did not show dependence on both the nature of the film and the time exposition in the electrolyte. The shape of the impedance spectra in the 10 mHz–10 kHz frequency (f) range corresponds to that of a capacitive semicircle, i.e. the data can be analyzed in terms of an RC parallel combination in series with an ohmic resistance R_Ω, according to the transfer function [35]

$$Z(j\omega) = R_\Omega + \frac{R}{1 + j\omega CR} \tag{5}$$

where $\omega = 2\pi f$. The high-frequency limit R_Ω corresponds to the ohmic resistance of the electrolyte, whereas R and C are the resistance and the capacitance, respectively, of the passive film. The resistance to the corrosion process can be visualized in terms of the oxide resistance defined at the limit of lower frequencies, that is $R = R_{ox} = \lim_{\omega\to 0}[-Z(j\omega)]$. Figures 5a and 6a show the complex-plane (or Nyquist) representation of the impedance data, whereas Figs. 5b and 6b show the respective Bode plots (impedance modulus $|Z|$ vs. $\log f$ and phase angle Θ vs. $\log f$). The only capacitive semicircle appearing in the Nyquist diagrams as well as the sharp maximum in the phase angle plots are strong evidences that a single and compact layer of the anodic oxide is passivating the alloy and that the oxide layer is the main responsible for the impedance response. As the impedance spectra shapes were not affected by the HA film, this is one more evidence that only a very thin layer of hydroxyapatite was electrodeposited onto the thicker oxide film. Different EIS data were reported by Souto et al. [36] for a very thick HA film deposited by plasma spraying on a Ti-6Al-4V alloy. For this case, two-layer models described well the EIS behavior of the electrode, considering a porous and thick ceramic film coating the alloy/open circuit oxide substrate.

For the Ti-13Nb-13Zr alloy, the experimental EIS spectra were satisfactorily described by Eq. (5) after an appropriate choice of parameters was made using a complex non-linear least square algorithm [37]; the resulting fitted impedance data are depicted as full symbols in Figs. 5 and 6. The calculated values of the parameters R_{ox} and C, obtained for the alloy with different coatings, are

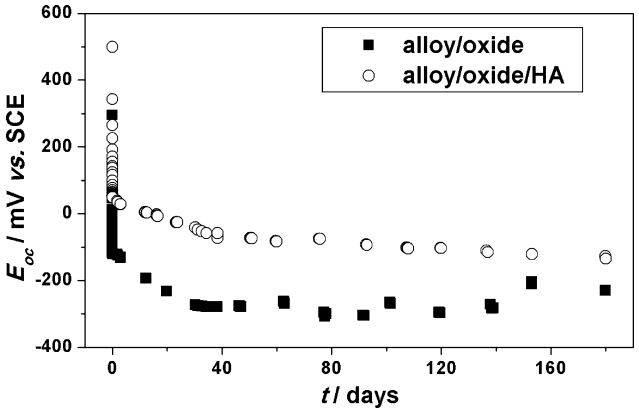

Fig. 4 Open-circuit potential versus time for the Ti-13Nb-13Zr alloy coated with either its anodic oxide film (alloy/oxide) or hydroxyapatite overlaying this oxide film (alloy/oxide/HA), in a PBS solution for up to 180 days

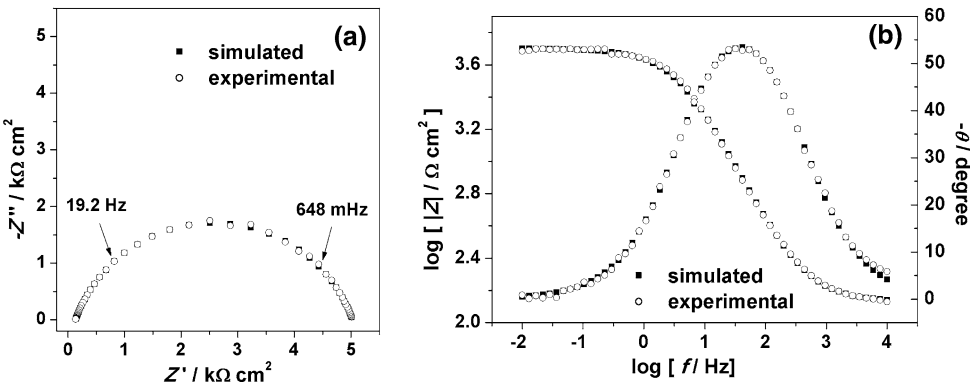

Fig. 5 Electrochemical impedance spectra obtained at 2 V (vs. SCE) for the Ti-13Nb-13Zr/oxide electrode, after 20 days of immersion in a PBS solution: (**a**) Nyquist diagram; (**b**) Bode diagram

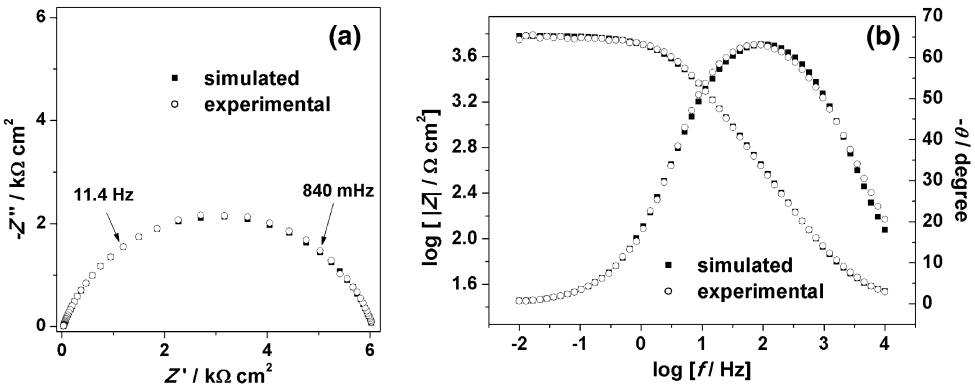

Fig. 6 Electrochemical impedance spectra obtained at 2 V (vs. SCE) for the Ti-13Nb-13Zr/oxide/HA electrode, after 180 days of immersion in a PBS solution: (**a**) Nyquist diagram; (**b**) Bode diagram

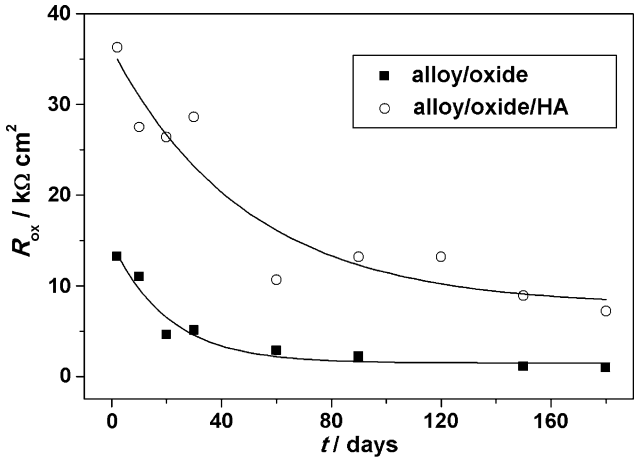

Fig. 7 Values of R_{ox} as a function of time, obtained from electrochemical impedance spectra similar to the ones in Figs. 4 and 5 for the Ti-13Nb-13Zr alloy coated with either its anodic oxide film (alloy/oxide) or hydroxyapatite overlaying this oxide film (alloy/oxide/HA), in a PBS solution for up to 180 days

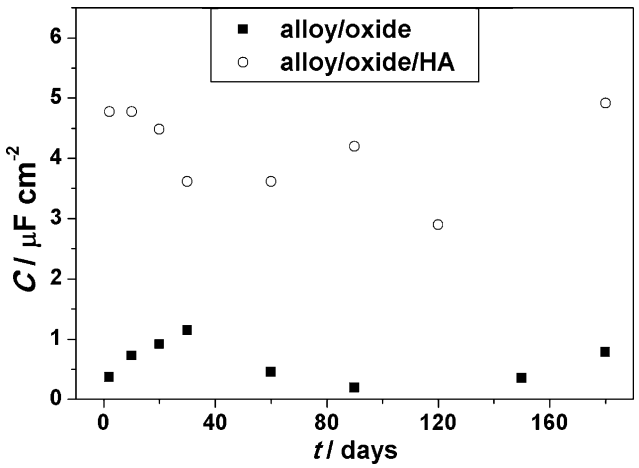

Fig. 8 Values of C as a function of time, obtained from electrochemical impedance spectra similar to the ones in Figs. 4 and 5 for the Ti-13Nb-13Zr alloy coated with either its anodic oxide film (alloy/oxide) or hydroxyapatite overlaying this oxide film (alloy/oxide/HA), in a PBS solution for up to 180 days

shown in Figs. 7 and 8, respectively, as a function of the immersion time in the PBS solution.

For either film coating (oxide or oxide/HA), the decrease of the R_{ox} values presented in Fig. 7 indicates that the corrosion process is enhanced after the alloy is immersed in the saline solution. In previous reports we already demonstrated that physiological solutions containing chloride ions (Ringer and PBS) are prone to break the stability of the passive oxides on Ti-50Zr and Ti-13Nb-13Zr alloys [17]; the same happened when the Ti-6Al-4V alloy was exposed to chloride-ion solutions [38]. Therefore, the sharp decrease of the resistance values in the first 30 days of immersion of the alloy in the PBS solution should be expected. Nevertheless, even after 180 days the quasi-stationary resistance value (>2 kΩ cm^2) is still high enough to maintain the corrosion of the Ti-13Nb-13Zr alloy at a low level in the physiological medium. On the other hand, R_{ox} values are systematically higher when HA is deposited on the alloy/oxide electrode, which means a beneficial effect towards protecting the alloy from corrosion. In either case, a decrease in the resistance values with the elapsed time may be related to some changes in the passive film like point-defect rearrangements and surface flaws with electrolyte penetration. However, these assumptions should be carefully investigated by other techniques.

The capacitance values, presented in Fig. 8, do not vary significantly with the immersion time of the respective electrodes in the PBS solution. Since the capacitance can be related to the area of the film/solution interface, these results are an indication that the dissolution process on both films (oxide and oxide/HA) occurred evenly and that the films kept the same average area in contact with the PBS solution.

4 Conclusions

Films of hydroxyapatite were successfully obtained by electrodeposition at a constant cathodic current on the

fresh-polished Ti-13Nb-13Zr alloy and on the alloy already passivated by its anodically grown oxide film. Results of open-circuit potential and electrochemical impedance spectroscopy measurements indicated that the HA coating positively affects the electrochemical properties of the alloy/oxide samples immersed in PBS solution.

The shift towards more positive open-circuit potentials and the increased resistance values when the alloy/oxide electrodes were coated with HA are strong evidences that the HA coating offers an extra protection against corrosion of the passive Ti-13Nb-13Zr alloy. This means that the as-prepared HA film, besides its well-known property of osteointegration improvement, seems to present the additional property of increasing the biomaterial stability.

Acknowledgements Financial support and scholarships from the Brazilian funding agencies CNPq (Conselho Nacional de Desenvolvimento Científico e Tecnológico) and CAPES (Coordenação de Aperfeiçoamento de Pessoal de Nível Superior) are gratefully acknowledged.

References

1. C.V. D'Alkaine, L.M.M. Souza, F.C. Nart, Corros. Sci. **34**, 117 (1993). doi:10.1016/0010-938X(93)90263-G
2. M.M. Lohrengel, Electrochim. Acta **39**, 1265 (1994). doi:10.1016/0013-4686(94)E0046-3
3. C.E.B. Marino, E.M. Oliveira, R.C. Rocha-Filho, S.R. Biaggio, Corros. Sci. **43**, 1465 (2001). doi:10.1016/S0010-938X(00)00162-1
4. Y. Okazaki, S. Rao, T. Tateishi, Y. Ito, Mater. Sci. Eng. A **243**, 250 (1998). doi:10.1016/S0921-5093(97)00809-5
5. M. Niinomi, D. Kuroda, K. Fukunaga, M. Morinaga, Y. Kato, T. Yashiro, A. Suzuki, Mater. Sci. Eng. A **263**, 193 (1999). doi:10.1016/S0921-5093(98)01167-8
6. M.C. Bottino, P.G. Coelho, M. Yoshimoto, B. König Jr, V.A.R. Henriques, A.H.A. Bressiani, J.C. Bressiani, Mater. Sci. Eng. C **28**, 223 (2008). doi:10.1016/j.msec.2006.12.014
7. M. Pourbaix, Biomaterials **5**, 122 (1984). doi:10.1016/0142-9612(84)90046-2
8. K. Wang, Mater. Sci. Eng. A **213**, 134 (1996). doi:10.1016/0921-5093(96)10243-4
9. E. Kobayashi, S. Matsumoto, T. Yoneyama, H. Hamanaka, J. Biomed. Mater. Res. **29**, 943 (1995). doi:10.1002/jbm.820290805
10. M.F. López, A. Gutiérrez, J.A. Jiménez, Surf. Sci. **482**, 300 (2001). doi:10.1016/S0039-6028(00)01005-0
11. M.A. Khan, R.L. Williams, D.F. Williams, Biomaterials **20**, 631 (1999). doi:10.1016/S0142-9612(98)00217-8
12. M.A. Khan, R.L. Williams, D.F. Williams, Biomaterials **20**, 765 (1999). doi:10.1016/S0142-9612(98)00229-4
13. M.F. López, A. Gutiérrez, J.A. Jiménez, Electrochim. Acta **47**, 1359 (2002). doi:10.1016/S0013-4686(01)00860-X
14. N.T.C. Oliveira, S.R. Biaggio, R.C. Rocha-Filho, N. Bocchi, J. Braz. Chem. Soc. **13**, 463 (2002)
15. N.T.C. Oliveira, S.R. Biaggio, R.C. Rocha-Filho, N. Bocchi, J. Biomed. Mater. Res. A **74**, 397 (2005). doi:10.1002/jbm.a.30352
16. N.T.C. Oliveira, S.R. Biaggio, S. Piazza, C. Sunseri, F. Di Quarto, Electrochim. Acta **49**, 4563 (2004). doi:10.1016/j.electacta.2004.04.042
17. N.T.C. Oliveira, E.A. Ferreira, L.T. Duarte, S.R. Biaggio, R.C. Rocha-Filho, N. Bocchi, Electrochim. Acta **51**, 2068 (2006). doi:10.1016/j.electacta.2005.07.015
18. Y. Abe, T. Kokubo, T. Yamamuro, J. Mater. Sci.: Mater. Med. **1**, 233 (1990). doi:10.1007/BF00701082
19. T. Brendel, A. Engel, C. Russel, J. Mater. Sci.: Mater. Med. **3**, 175 (1992). doi:10.1007/BF00713445
20. Y.H. Yun, V.T. Turitto, K.P. Daigle, P. Kovacs, J.A. Davidson, S.M. Slack, J. Biomed. Mater. Res. **32**, 77 (1996). doi:10.1002/(SICI)1097-4636(199609)32:1<77::AID-JBM9>3.0.CO;2-M
21. M. Shirkhanzadeh, J. Mater. Sci. Lett. **12**, 16 (1993)
22. J.H. Park, D.Y. Lee, K.T. Oh, Y.K. Lee, K.M. Kim, K.N. Kim, Mater. Lett. **60**, 2573 (2006). doi:10.1016/j.matlet.2005.07.091
23. J.H. Park, Y.K. Lee, K.M. Kim, K.N. Kim, Surf. Coat. Tech. **195**, 252 (2005). doi:10.1016/j.surfcoat.2004.08.185
24. S. Ban, S. Maruno, N. Arimoto, A. Hanada, J. Hasegawa, J. Biomed. Mater. Res. **36**, 9 (1997). doi:10.1002/(SICI)1097-4636(199707)36:1<9::AID-JBM2>3.0.CO;2-P
25. J.M. Zhang, C.J. Lin, Z.D. Feng, Z.W. Tian, J. Electroanal. Chem. **452**, 235 (1998). doi:10.1016/S0022-0728(98)00107-7
26. S.K. Yen, C.M. Lin, Mater. Chem. Phys. **77**, 70 (2002). doi:10.1016/S0254-0584(01)00562-4
27. S.K. Yen, M.C. Kuo, Mater. Sci. Eng. C **20**, 153 (2002). doi:10.1016/S0928-4931(02)00026-7
28. W.J.A. Dhert, P. Thomsen, A.K. Blomgren, M. Esposito, L.E. Ericson, A.J. Verbout, J. Biomed. Mater. Res. **41**, 574 (1998). doi:10.1002/(SICI)1097-4636(19980915)41:4<574::AID-JBM9>3.0.CO;2-9
29. V.S. Komlev, S.M. Barinov, J. Mater. Sci.: Mater. Med. **13**, 295 (2002). doi:10.1023/A:1014015002331
30. C.J. Damien, J.R. Parsons, J.J. Benedict, D.S. Weisman, J. Biomed. Mater. Res. **24**, 639 (1990). doi:10.1002/jbm.820240602
31. M.A. Lopez-Heredia, P. Weiss, P. Layrolle, J. Mater. Sci.: Mater. Med. **18**, 381 (2007). doi:10.1007/s10856-006-0703-8
32. A. Rakngarm, Y. Miyashita, Y. Mutoh, J. Mater. Sci.: Mater. Med. **19**, 1953 (2008). doi:10.1007/s10856-007-3285-1
33. Y.M. Song, D.Y. Shan, E.H. Han, Mater. Lett. **62**, 3276 (2008). doi:10.1016/j.matlet.2008.02.048
34. S.Y. Yu, J.R. Scully, Corrosion **53**, 965 (1997)
35. S.R. Biaggio, R.C. Rocha-Filho, J.R. Vilche, F.E. Varela, L.M. Gassa, Electrochim. Acta **42**, 1751 (1997). doi:10.1016/S0013-4686(96)00375-1
36. R.M. Souto, M.M. Laz, R.L. Reis, Biomaterials **24**, 4213 (2003). doi:10.1016/S0142-9612(03)00362-4
37. B.A. Boukamp, Solid State Ionics **18**, 136 (1986). doi:10.1016/0167-2738(86)90100-1
38. C.E.B. Marino, S.R. Biaggio, R.C. Rocha-Filho, N. Bocchi, Electrochim. Acta **51**, 6580 (2006). doi:10.1016/j.electacta.2006.04.051